JOURNAL OF THERMOPHYSICS AND HEAT TRANSFER
Vol. 24, No. 4, October–December 2010

Thermal Performance Analysis of Space Debris Protection Enhanced Multilayer Perforated Insulation

Wen-long Cheng,* Hui Li,† and Na Liu‡
University of Science and Technology of China, 230027 Hefei, People's Republic of China
Jia-rong Huang§ and Hai-ying Han¶
China Academy of Space Technology, 100094 Beijing, People's Republic of China
and
Shi Pang†
University of Science and Technology of China, 230027 Hefei, People's Republic of China

DOI: 10.2514/1.48816

The space debris protection level of multilayer perforated insulation component is enhanced by inserting strength-enhanced materials (e.g., Kevlar fiber, high-strength polyethylene) in this study. The thermal properties of multilayer perforated insulation and its associated materials were measured. An analysis model for the thermal performance of the multilayer perforated insulation was developed by energy balance method, and a contact coefficient was introduced to modify the model, due to the separation caused by the deflation of the multilayer perforated insulation between the reflective screens and the mesh solid spacers. The results calculated from the modified model coincide well with the experimental data. The effective thermal conductivities of the space debris protection enhanced multilayer perforated insulation by inserting Kevlar fabric and high-strength polyethylene were investigated by the modified model. The analysis results show that the effective thermal conductivities are greatly affected by the layers of the strength-enhanced material in that they increase linearly with the layers but are influenced little by the inserted position. However, the effective emissivities of the multilayer perforated insulation are affected little by the types, positions, and layers of the inserted reinforcing materials.

Nomenclature

A	=	area of sample, m^2
d	=	distance between adjacent screens, m
f	=	contact coefficient
k_c	=	effective thermal conductivity between adjacent reflective screens, $W \cdot m^{-1} \cdot K^{-1}$
k_{eff}	=	effective thermal conductivity of sample, $W \cdot m^{-1} \cdot K^{-1}$
k_s	=	thermal conductivity of mesh solid spacer, $W \cdot m^{-1} \cdot K^{-1}$
Q	=	heating power of heating plate, W
R_g	=	electric resistance, Ω
T	=	temperature, K
U	=	voltage, V
δ	=	thickness of sample, m
ε	=	emissivity of reflective screen
ε_{eff}	=	effective emissivity of sample
ζ	=	porosity of the mesh solid
ξ	=	perforated rate of reflective screen
σ	=	Stefan–Boltzmann constant

I. Introduction

A MULTILAYER perforated insulation (MLPI) component is widely used in thermal control of spacecraft, due to its excellent insulation performance, low density, and so on [1,2]. A numerical model was presented to investigate the combined radiation/conduction heat transfer of MLPI at high temperatures in which the thermal radiation was modeled by using a two-flux approximation, and the thermal conduction was modeled by using techniques for high-porosity materials [3]. A layer-by-layer heat transfer model was developed to analyze the heat transfer of MLPI used for thermal isolation under high-vacuum case, and the deviations of the calculated thermal conductivities were within 30% compared to the experimental data [4]. MLPI was treated as a kind of thermal coating with low solar absorptivity and low infrared emissivity by means of an equivalent method, and the error of the equivalent was analyzed [5]. The effective emittance for Cassini MLPI blankets and the heat loss near the seams were investigated by experimental method [6]. The steady and transient models for the thermal performance of MLPI were established based on the energy balance equations of the reflective screens, and the effects of layer density on the effective thermal conductivities, heat flux, and temperature distribution were analyzed [7–9]. The heat transfer through MLPI was studied experimentally, and it was concluded that the shape and structure played an important role in the thermal performance of MLPI [10].

While a spacecraft runs in the meteoroid and orbital debris environment, the on-orbit impacts by this high-speed debris can lead to catastrophic failure for the spacecraft. The perforation resistance against the impacts of dual-wall structural systems fabricated with monolithic bumper plates and corrugated bumper plates was studied [11]. In general, MLPI is coated on the outside of a spacecraft and exposed to the orbital environment, and therefore it is highly susceptible to the impacts of pieces of space debris. Some methods, including increasing MLPI layers and inserting reinforcing materials (such as β fabric, Kevlar fiber, Nextel ceramic blanket, and so on) into the MLPI, are developed to improve the debris protection performance against the impacts. However, little literature on the thermal performance of space debris protection enhanced (SDPE) MLPI (SDPE-MLPI) has been found so far.

This paper focuses on the thermal performance of a space debris protection enhanced MLPI by inserting reinforcing materials. A

Received 8 January 2010; revision received 15 July 2010; accepted for publication 15 July 2010.

*Associate Professor, Department of Thermal Science and Energy Engineering, Anhui.
†Undergraduate, Department of Thermal Science and Energy Engineering, Anhui.
‡Ph.D. Candidate, Department of Thermal Science and Energy Engineering, Anhui.
§Senior Engineer.
¶Engineer.

prediction model for the thermal performance of SDPE-MLPI is developed based on energy balance and modified by comparison with the experimental results obtained in this study. The effects of the types, layers, and inserted positions of the reinforcing materials on the thermal performance are analyzed by the model.

II. Measurement of Thermal Properties of MLPI

A. Measurement of Thermal Parameters of the Associated Materials

The MLPI mainly consists of fire-retardant fabric for coating, double-sided aluminized polyester film, mesh solid spacer, and inserted reinforcing material for enhancement of space debris protection (high-strength polyethylene and Kevlar fabric in this study). The thermal conductivities of these associated materials (except mesh solid spacers) were measured by Hot Disk Thermal Constants Analyzer with error of ±3%. The measured results are listed in Table 1.

B. Measurement of Thermal Performance of the MLPI

The principle of the measurement for the thermal performance of MLPI is shown in Fig. 1. The test piece is composed of a heating plate and two identical MLPI samples placed symmetrically on each side of the heating plate. The effective thermal conductivity k_{eff} and the effective emissivity ε_{eff} of the sample can be calculated as follows:

$$k_{\text{eff}} = \frac{Q\delta}{2\Delta T \cdot A} \tag{1}$$

$$\varepsilon_{\text{eff}} = \frac{Q}{2A\sigma(T_1^4 - T_2^4)} \tag{2}$$

where Q is the heating power of the heating plate; δ and A are the thickness and area of the samples, respectively; and ΔT is the temperature difference between the two sides of the samples.

To simulate the space environment of low temperature and high vacuum, the thermal performance of MLPI was tested in a vacuum tank with an effective volume of 98 liters. The structure of the vacuum tank is shown in Fig. 2, and the equipment is shown in Fig. 3. The inner wall of the tank is coated by 3M black paint, which can be assumed to be a blackbody. The tank can be vacuumized to a vacuity of about 10^{-5} Pa by a group of vacuum pumps. The inner wall of the tank can be cooled by filling liquid nitrogen continuously, and its temperature can be maintained at about 100 K.

Two kinds of MLPI with 20 layers were measured in this study. One is normal MLPI and the other is a SDPE-MLPI, made by inserting a layer of Kevlar fabric as the reinforcing material. Both of the MLPIs were assembled by reflective screen and mesh solid spacer in turn (shown in Fig. 4). The reflective screens were double-sided aluminized polyester film, and the mesh solid spacers were high-silica glass fiber. The outer surfaces of the MLPIs were coated with a layer of fire-retardant fabric. For the SDPE-MLPI, one layer of Kevlar fabric was inserted between the fire-retardant fabric and the outermost reflective screen to improve space debris protection performance. The size of the test piece was 200 × 200 mm.

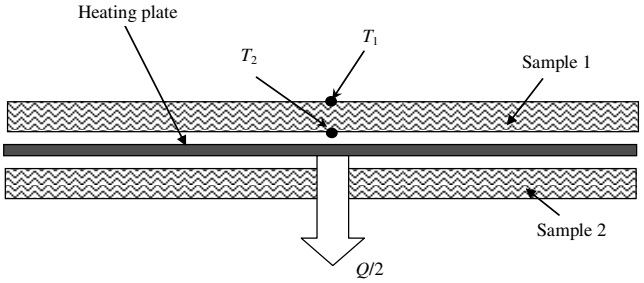

Fig. 1 Schema chart of measurement principle.

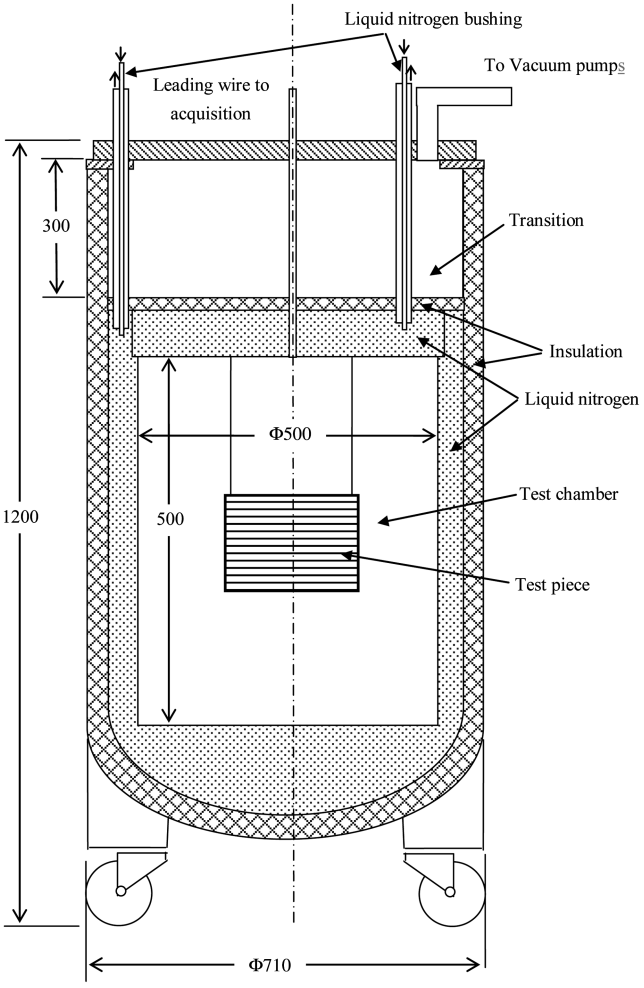

Fig. 2 Sketch of the vacuum tank.

At first, the test piece was enclosed in the vacuum tank, and the vacuum tank was vacuumized by the vacuum pumps. After being vacuumized to a vacuity of about 10^{-4} Pa, liquid nitrogen was filled to cool the inner wall of the vacuum tank and the heating plate was

Table 1 MLPI component material properties and geometric parameters

		Thermal property		Geometric parameters	
Part	Material	Conductivity[a]	Emissivity	Thickness, mm	Porosity
Reflecting screen	Double-sided aluminized polyester film	0.012	0.022	0.006	0.011[b]
Mesh spacer	High-silica glass fiber	0.058	——	0.10	0.995[c]
External coating	Fire-retardant fabric	0.072	0.83	0.115	——
Enhanced material	High-strength polyethylene	0.093	——	0.40	——
Enhanced material	Kevlar	0.057	——	0.30	——

[a]Data are measured with a hot disk.
[b]Reflective screen's drilling rate.
[c]Mesh rate of the spacer solids between screens.

Fig. 3 Photograph of the vacuum tank.

heated by a direct current supply. The temperatures of the test piece and inner wall of the tank were measured by thermocouples. The whole equipment reached a steady state after about 18 h; thereafter, the temperatures did not change with time.

Because the heating plate is heated by a direct current supply, Eqs. (1) and (2) can be rewritten as

$$k_{\text{eff}} = \frac{U^2\delta}{2R_g\Delta T \cdot A} \tag{3}$$

$$\varepsilon_{\text{eff}} = \frac{U^2}{2R_gA\sigma(T_1^4 - T_2^4)} \tag{4}$$

where U is the voltage supplied to the heating plate, and R_g is the electric resistance of the heating plate. Therefore, the effective thermal conductivity k_{eff} and the effective emissivity ε_{eff} of the MLPI can be calculated by Eqs. (3) and (4), respectively.

The experimental uncertainties of effective conductivity and effective emissivity can be obtained by error propagation formulas (5) and (6) derived from Eqs. (3) and (4), respectively:

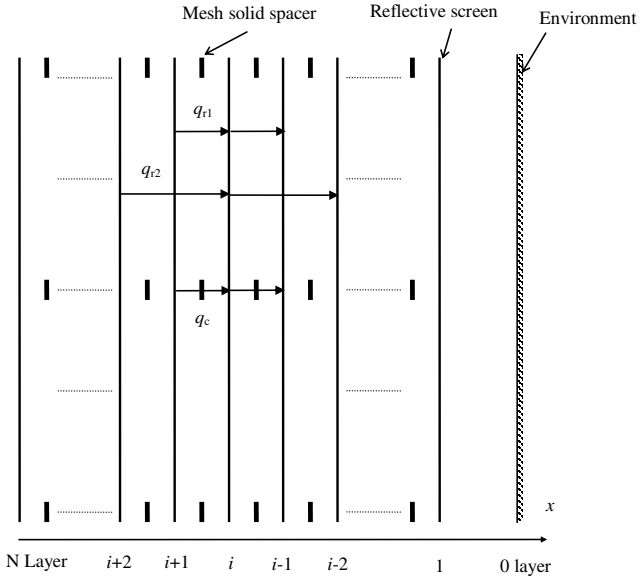

Fig. 4 Physical model of the heat transfer of MLPI.

The experimental conditions and measurement results for the two kinds of MLPI are listed in Table 2. The effective thermal conductivities of the normal MLPI and SDPE-MLPI were 6.3×10^{-4} and 6.7×10^{-4} $\text{W} \cdot \text{m}^{-1} \cdot \text{K}^{-1}$, with uncertainties of 0.3×10^{-4} and 0.4×10^{-4} $\text{W} \cdot \text{m}^{-1} \cdot \text{K}^{-1}$, respectively, and the effective emissivities were 0.023 and 0.022, with uncertainties of 0. 004 and 0.004, respectively.

III. Thermal Analysis Model for MLPI

Considering the expensive cost of the experiments for the thermal performance of MLPI, it is necessary to set up an analysis model to study the effects of the reinforcing materials inserted on the thermal performance of MLPI in detail.

The heat transfer mechanism of the MLPI, including the radiations between the reflective screens, the conductions through the mesh solid spacers, and so on, is very complex. To simplify the thermal model, some assumptions are made as follows:

1) For sufficiently low pressure of the rarefied gas between the reflective screens, both the convection and conduction occurring in the gas are much less than the thermal conduction through the mesh solid spacers between the reflective screens; therefore, the convection and conduction occurring in the gas can be ignored.

2) The heat transfer process can be simplified as one-dimensional heat transfer in the x direction, due to a very large width/thickness ratio in the practical application of MLPI.

3) According to the above measurement results, the thermal resistance caused by the reflective screens is less than 1‰ of the overall thermal resistance for a 20-layer MLPI. Therefore, the thermal resistance contributed by the reflective screens can be ignored and the reflective screens can be assumed to be isothermal.

4) It is difficult to determine the values of the thermal contact resistances between the mesh solid spacers and the reflective screens,

$$\delta k_{\text{eff}} = \sqrt{\left(\frac{U\delta}{R_gA\Delta T}\,\mathrm{d}U\right)^2 + \left(\frac{U^2}{2R_gA\Delta T}\,\mathrm{d}\delta\right)^2 + \left(\frac{U^2\delta}{2R_g^2A\Delta T}\,\mathrm{d}R_{\text{g}}\right)^2 + \left(\frac{U^2\delta}{2R_gA^2\Delta T}\,\mathrm{d}A\right)^2 + \left(\frac{U^2\delta}{2R_gA\Delta T^2}\,\mathrm{d}T_1\right)^2 + \left(\frac{U^2\delta}{2R_gA\Delta T^2}\,\mathrm{d}T_2\right)^2} \tag{5}$$

$$\delta\varepsilon_{\text{eff}} = \sqrt{\left(\frac{U}{R_gA\sigma\Delta T^{(4)}}\,\mathrm{d}U\right)^2 + \left(\frac{U^2}{2R_g^2A\sigma\Delta T^{(4)}}\,\mathrm{d}R_{\text{g}}\right)^2 + \left(\frac{U^2}{2R_gA^2\sigma\Delta T^{(4)}}\,\mathrm{d}A\right)^2 + \left(\frac{2U^2T_1^3}{R_gA\sigma\Delta T^{(4)2}}\,\mathrm{d}T_1\right)^2 + \left(\frac{2U^2T_2^3}{R_gA\sigma\Delta T^{(4)2}}\,\mathrm{d}T_2\right)^2} \tag{6}$$

where $\Delta T = T_1 - T_2$, and $\Delta T^{(4)} = T_1^4 - T_2^4$.

due to their uncertainties. Therefore, the thermal contact resistances are not taken into consideration at first in this model. The error caused by the assumption will be modified by a contact coefficient introduced later.

5) The outermost layer, next to the space environment, is labeled as the first layer of MLPI. In turn, the innermost layer, next to the spacecraft, is labeled as the Nth layer. The Nth layer is assumed to be isothermal.

6) The environment that is labeled as layer 0 in this study is assumed to be a blackbody with a constant temperature. In the real space environment case, the environmental temperature is about 4 K. However, in the experimental case, the environmental temperature (temperature of the vacuum tank wall) is about 100 K.

Based on the above assumptions, the physical model for the heat transfer process of MLPI is shown in Fig. 4. For a reflective screen, the heat transfer process mainly includes the thermal conduction q_c between the adjacent reflective screens through the mesh solid spacers, the thermal radiation q_{r1} between the adjacent reflective screens, and the thermal radiation q_{r2} between the two reflective screens interval of the adjacent screen through the small holes perforated in the adjacent screen. The heat fluxes reaching the ith layer are as follows:

1) The thermal conduction $q_{c(i+1,i)}$ from layer $(i+1)$ screen through the mesh solid spacer is

$$q_{c(i+1,i)} = k_c \frac{T_{i+1} - T_i}{d} \tag{7}$$

2) The thermal radiation $q_{r1(i+1,i)}$ from layer $(i+1)$ screen is

$$q_{r1(i+1,i)} = \frac{\sigma(T_{i+1}^4 - T_i^4)}{2/\varepsilon - 1}(1-\xi) \tag{8}$$

3) The thermal radiation $q_{r2(i+2,i)}$ from the layer $i+2$ screen through the small holes perforated in the layer $i+1$ screen is

$$q_{r2(i+2,i)} = \xi \frac{\sigma(T_{i+2}^4 - T_i^4)}{2/\varepsilon - 1} \tag{10}$$

where k_c is the effective thermal conductivity between the adjacent reflective screens that can be expressed by

$$k_c = (1-\zeta)k_s \tag{11}$$

k_s is the thermal conductivity of the mesh solid spacer, ζ is the porosity of the mesh solid spacer between the screens, d is the distance between the adjacent screens, ξ is the perforated rate of the reflective screens, ε is the emissivity of the reflective screens, and σ is the Stefan–Boltzmann constant equal to $5.670 \times 10^{-8}\ \mathrm{W \cdot m^{-2} \cdot K^{-4}}$. Corresponding to $q_{c(i+1,i)}$, $q_{r1(i+1,i)}$, and $q_{r2(i+2,i)}$, the heat fluxes leaving from the ith layer ($q_{c(i,i-1)}$, $q_{r1(i,i-1)}$, and $q_{r2(i,i-2)}$) can be obtained easily by the same method.

For the ith layer, the energy balance equation can be expressed as

$$[q_{c(i+1,i)} = q_{r1(i+1,i)} + q_{r2(i+2,i)}] - [q_{c(i,i-1)} + q_{r1(i,i-1)} + q_{r2(i,i-2)}] = 0 \tag{12}$$

Incorporating $q_{c(i+1,i)}$, $q_{r1(i+1,i)}$ and $q_{r2(i+2,i)}$ and $q_{c(i,i-1)}$, $q_{r1(i,i-1)}$, and $q_{r2(i,i-2)}$ into Eq. (12), the energy balance equation becomes

$$\frac{(1-\xi)\sigma}{2/\varepsilon - 1}(T_{i+1}^4 - 2T_i^4 + T_{i-1}^4) + \frac{\xi\sigma}{2/\varepsilon - 1}(T_{i+2}^4 - 2T_i^4 + T_{i-2}^4) + \frac{k_c}{d}(T_{i+1} - 2T_i + T_{i-1}) = 0 \tag{13}$$

According to assumption 6, the environment labeled as layer 0 is assumed to be a blackbody with a constant temperature T_0. Therefore, the energy balance equation of layer 1 is

$$\frac{(1-\xi)\sigma}{2/\varepsilon - 1}(T_2^4 - T_1^4) - (1-\xi)\varepsilon\sigma(T_1^4 - T_0^4) + \frac{\xi\sigma}{2/\varepsilon - 1}(T_3^4 - T_1^4) + \frac{k_c}{d}(T_2 - T_1) = 0 \tag{14}$$

The energy balance equation of layer 2 is

$$\frac{(1-\xi)\sigma}{2/\varepsilon - 1}(T_3^4 - 2T_2^4 + T_1^4) + \frac{\xi\sigma}{2/\varepsilon - 1}(T_4^4 - T_2^4) + \frac{k_c}{d}(T_3 - 2T_2 + T_1) = 0 \tag{15}$$

The energy balance equation of the layer $N-1$ is

$$\frac{(1-\xi)\sigma}{2/\varepsilon - 1}(T_N^4 - 2T_{N-1}^4 + T_{N-2}^4) - \frac{\xi\sigma}{2/\varepsilon - 1}(T_{N-1}^4 - T_{N-3}^4) + \frac{k_c}{d}(T_N - 2T_{N-1} + T_{N-2}) = 0 \tag{16}$$

Layer N is assumed to be a constant-temperature surface.

IV. Contact Coefficient and Modified Thermal Analysis Model for MLPI

For the normal MLPI and the SDPE-MLPI, the effective thermal conductivities calculated from the model are 1.62×10^{-3} and $1.69 \times 10^{-3}\ \mathrm{W \cdot m^{-1} \cdot K^{-1}}$, respectively; however, the corresponding experimental results listed in Table 2 are 6.3×10^{-4} and $6.7 \times 10^{-4}\ \mathrm{W \cdot m^{-1} \cdot K^{-1}}$, respectively. It can be concluded that the effective thermal conductivities obtained by the model are much larger than the experimental results. The large errors between the theoretical values and the experimental values are induced by the deflation of the MLPI. During the experimental process, the air in the test chamber of the vacuum tank is extracted by the vacuum pumps at first, and the pressure in the test chamber drops down suddenly. However, the air contained in the MLPI is blocked from flowing out smoothly by the reflective screens, mesh solid spacers, reinforcing materials, and so on. Therefore, a pressure gradient exists in the MLPI during the deflation process. The pressure difference between the MLPI and the ambient may lead to the separation between the reflective screens and the mesh solid spacers. The thermal performances of the MLPI are greatly affected by the contact situation between the reflective screens and the mesh solid spacers, which is ignored in the presented model. Therefore, the presented model should be modified and the contact situation should be taken into consideration in the modified model.

To modify the presented model, a contact coefficient f is introduced in this study, which is defined as the ratio of A and A_0:

Table 2 Experiment conditions and results

	Environment condition		Sample size		Experimental condition				Experimental result	
Sample	T_0, K	P_0, 10^{-4} Pa	δ, m	A, m^2	U, V	R_g, Ω	T_1, K	T_2, K	k_{eff}, W·m^{-1}·K^{-1}	$\varepsilon_{\mathrm{eff}}$
Normal MLPI										
Tested value	77.0	5.8	0.0095	0.040	10.22	45.0	310.4	133.9	6.3×10^{-4}	0.023
Uncertainty	——	——	0.0002	0.003	0.01	0.1	1	1	0.3×10^{-4}	0.004
SDPE-MLPI										
Tested value	77.0	5.8	0.0098	0.040	10.22	45.0	313.7	150.7	6.7×10^{-4}	0.022
Uncertainty	——	——	0.0002	0.003	0.01	0.1	1	1	0.4×10^{-4}	0.004

$$f = \frac{A}{A_0} \tag{17}$$

where A is the actual contact area of the reflective screens and the mesh solid spacers, and A_0 is the ideal contact area at the full contact situation. In fact, the contact coefficient does not only indicate the separation situation between the reflective screens and the mesh solid spacers, it also indicates the thermal contact resistance between the reflective screens and the mesh solid spacers. Therefore, the effective thermal conductivity between the adjacent reflective screens described in Eq. (11) becomes

$$k_c = f(1-\zeta)k_s \tag{18}$$

For the normal MLPI and the SDPE-MPLI, the relationship of the effective thermal conductivity obtained by the modified model versus the contact coefficient f is shown in Fig. 5. Obviously, the effective thermal conductivity decreases linearly with f decreasing. For both the normal MLPI and the SDPE-MPLI, while the contact coefficient f is about 0.45, the effective thermal conductivities are in very good agreement with the experimental data of 6.3×10^{-4} and 6.7×10^{-4} W · m^{-1} · K^{-1}, respectively. It indicates that the contact coefficients of MLPIs are approximately equal under a similar experimental condition.

V. Thermal Performance of Debris Protection Enhanced MLPI

The thermal performance of the MLPIs is analyzed by the modified model. The MLPI with 20 layers is coated with the fire-retardant fabric; the innermost layer is considered as an isothermal panel with temperature 300 K, and the ambient temperature is 4 K. Two conditions of the contact coefficient, 1.0 and 0.45, are considered.

Four types of MLPI shown in Fig. 6 will be analyzed:

1) Normal MLPI has no inserted reinforcing material.

2) Outside-enhanced SDPE-MLPI has reinforcing material inserted between the outermost layer and the fire-retardant fabric.

3) Middle-enhanced SDPE-MLPI has the reinforcing material inserted in the middle part of layers of the MLPI.

4) Inside-enhanced SDPE-MLPI has the reinforcing material inserted in the innermost layer.

For the three types of SDPE-MLPI, high-strength polyethylene and Kevlar fabric are used as the reinforcing material. The relationships between the effective thermal conductivities of the three types of SDPE-MLPI versus the layers of the inserted reinforcing materials are shown in Figs. 7a and 7b, and the contact coefficient f is assumed to be 1.0 and 0.45, respectively. From Fig. 7, the following conclusions can be obtained,

1) For the SDPE-MLPIs, the effective thermal conductivities are larger than that of the normal MLPI and increase linearly with the layers of the reinforcing materials. It can be explained by the fact that the thermal conductivities of the reinforcing materials (Kevlar fabric and polyethylene) inserted into the SDPE-MLPIs are much larger than that of the normal MLPI.

2) The effective thermal conductivity of the SDPE-MLPI inserted with Kevlar fabric is smaller than that of the SDPE-MLPI inserted with high-strength polyethylene under the same condition, because both the thermal conductivity and thickness of the Kevlar fabric are smaller than those of the high-strength polyethylene.

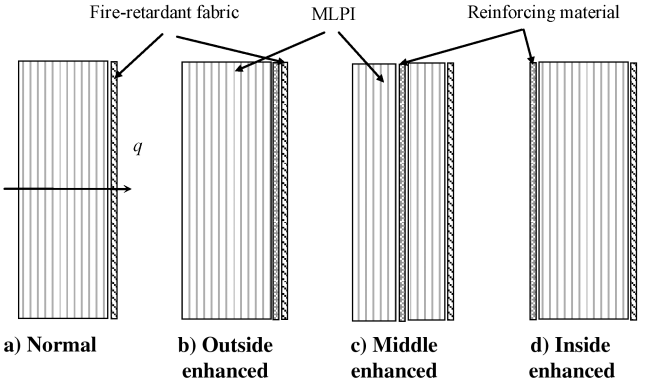

Fig. 6 Types of MLPI.

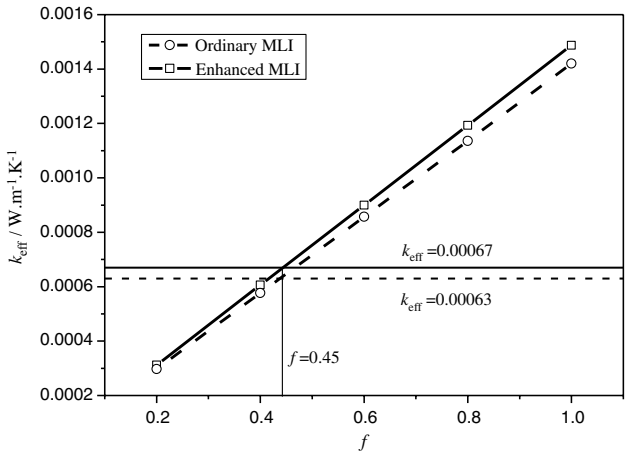

Fig. 5 Relationship between effective thermal conductivity and contact coefficient.

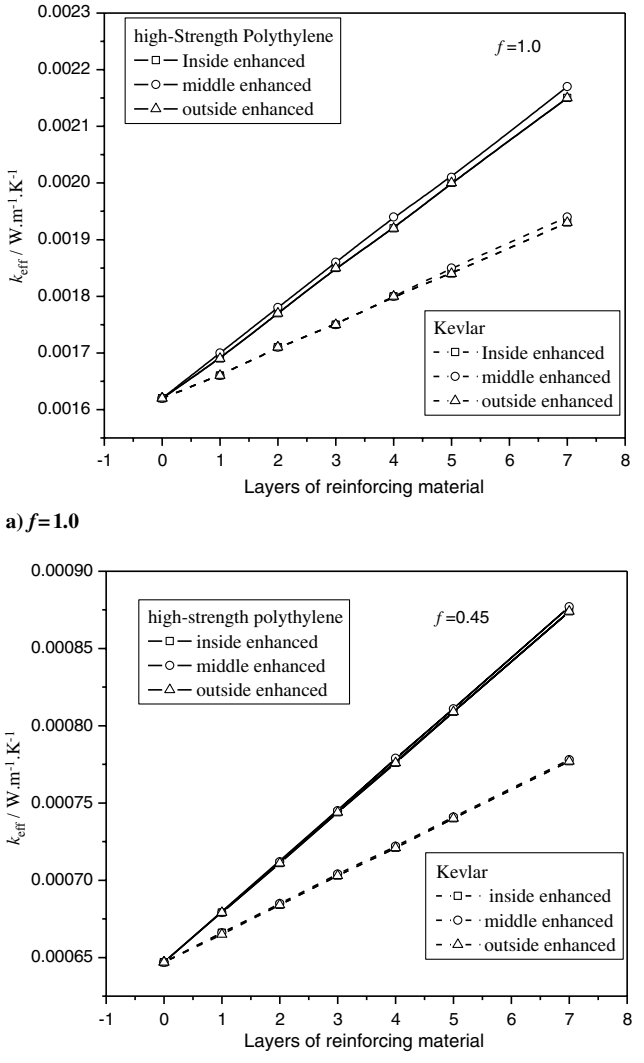

Fig. 7 Relationship of effective thermal conductivity versus layers of inserted material.

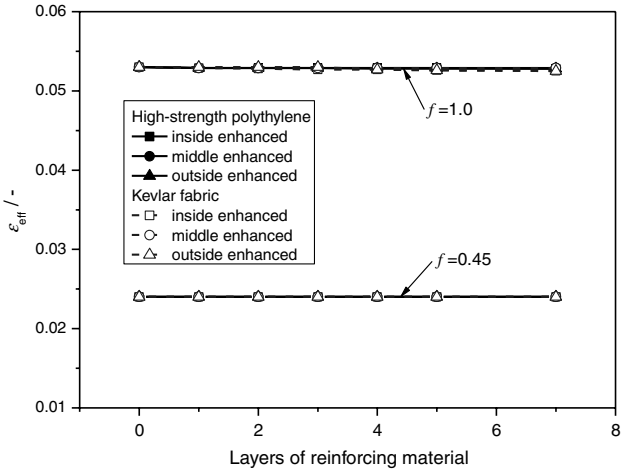

Fig. 8 Relationship of effective emissivity versus layers of inserted reinforcing material.

3) For a certain kind of reinforcing material, the position inserted into the MLPI has little influence on the thermal conductivity, which can be easily explained by the series connection theory of thermal resistances.

The relationships of the effective emissivities of the three types of SDPE-MLPI versus the layers of the inserted reinforcing materials are shown in Fig. 8. It shows that the effective emissivities of the SDPE-MLPI have little relation with the inserted position, type, and layers of the reinforcing materials, but are influenced greatly by the contact coefficient f. While the contact coefficient f decreases from 1.0 to 0.45, the effective emissivities of the SDPE-MLPI drop down from 0.053 to 0.024. This is because the overall thermal resistance of SDPE-MLPI is connected in series by three parts: the thermal resistances of the MLPI, the thermal resistances of the inserted reinforcing material, and the contact thermal resistances. The contact thermal resistance is directly influenced by the contact coefficient f. However, the thermal resistance caused by the inserted reinforcing material can be neglected, due to the very small thickness and very large thermal conductivity of the reinforcing material, compared with the MLPI.

VI. Conclusions

This paper established a thermal analysis model for MLPI to investigate the influences of the inserted reinforcing materials on the thermal performance of SDPE-MLPI. The effective thermal conductivities and emissivities of the MLPIs were measured in a vacuum container with low temperature, and the model presented was modified by the experimental results. The conclusions can be summarized as follows:

1) According to the experimental results, the effective thermal conductivities of the normal MLPI with 20 layers and the SDPE-MLPI are 6.3×10^{-4} and 6.7×10^{-4} $\mathrm{W \cdot m^{-1} \cdot K^{-1}}$, and the effective emissivities are 0.023 and 0.022, respectively.

2) A contact coefficient is introduced to modify the model. The contact coefficient not only indicates the separation of reflective screens and the mesh solid spacers caused by deflation of the MLPI, but also indicates the thermal contact resistance.

3) The effective thermal conductivities of the SDPE-MLPI are larger than that of the normal MLPI and increase with the layers of the reinforcing materials inserted into the MLPI.

4) The effective emissivities of the MLPI have little relation with the inserted position, type, and layers of the reinforcing materials.

5) Both the effective thermal conductivities and effective emissivities of MLPI are influenced greatly by the contact coefficient f.

Acknowledgment

The authors would like to thank the National Science Foundation of China for the financial support (grant no. 50876096).

References

[1] Anderson, C. C., and Hattar, M. M., "Calorimetric Measurement of Thermal Control Surface at Geosynchronous Orbit," *Journal of Thermophysics and Heat Transfer*, Vol. 2, No. 2, 1988, pp. 145–151. doi:10.2514/3.78

[2] Kamran, D., "Thermal Analysis and Design Optimization of Multilayer Insulation for Reentry Aerodynamic Heating," *Journal of Spacecraft and Rockets*, Vol. 39, No. 4, 2002, pp. 509–514. doi:10.2514/2.3863

[3] Ma, Z.-H., Sun, Q., Wang, X.-J., and Wang, Y., "TPS Multi-Layer Insulation Thermal Analysis and Performance Study," *Journal of Astronautics*, Vol. 24, No. 5, 2003, pp. 17–20.

[4] Xiao, Z.-H., Wang, R.-S., Shi, Y.-M., and Gu, A.-Z., "Theoretical Analysis of Heat Transfer of High Vacuum Multi-Layers," *Vacuum Science and Technology*, Vol. 24, No. 2, 2004, pp. 113–117.

[5] Zhao, X., "Analysis of Equivalent Thermal Properties of MLI," *Spacecraft Engineering*, Vol. 17, No. 4, 2008, pp. 51–55.

[6] Edward, I. L., James, W. S., and Ronald, T. R., "Effective Emittance for Cassini Multilayer Insulation Blankets and Heat Loss near Seams," *Journal of Thermophysics and Heat Transfer*, Vol. 10, No. 2, 1996, pp. 357–363. doi:10.2514/3.795

[7] Li, P., and Cheng, H.-E., "Steady Numerical Simulation and Performance Analysis of Multilayer Perforated Insulation Material in Orbit," *Cryogenics and Superconductivity*, Vol. 34, No. 2, 2006, pp. 75–78, 132.

[8] Li, P., Xiao, Z.-J., and Cheng, H.-E., "Numerical Model Study of Thermal Analysis on Multilayer Perforated Insulation Material in Orbit," *Chinese Space Science Technology*, Vol. 26, No. 5, 2006, pp. 17–20.

[9] Li, P., and Cheng, H.-E., "Thermal Analysis and Performance Study for Multilayer Perforated Insulation Material Used in Space," *Applied Thermal Engineering*, Vol. 26, 2006, pp. 2020–2026. doi:10.1016/j.applthermaleng.2006.01.004

[10] Wei, W., Li, X.-D., Wang, R.-S., and Li, Y., "Effects of Structure and Shape on Thermal Performance of Perforated Multilayer Insulation Blankets," *Applied Thermal Engineering*, Vol. 29, 2009, pp. 1264–1266. doi:10.1016/j.applthermaleng.2008.06.024

[11] William, P. S., "Spacecraft Wall Design for Increased Protection Against Penetration by Orbital Debris Impacts," *AIAA Journal*, Vol. 29, No. 12, 1991, pp. 2207–2214. doi:10.2514/3.10861